Journal of Molecular Catalysis A: Chemical 352 (2012) 86–94

Contents lists available at SciVerse ScienceDirect

Journal of Molecular Catalysis A: Chemical

journal homepage: www.elsevier.com/locate/molcata

Diesel particulate matter combustion with CeO_2 as catalyst. Part I: System characterization and reaction mechanism

Martín S. Gross, María A. Ulla, Carlos A. Querini*

Instituto de Investigaciones en Catálisis y Petroquímica (INCAPE) – FIQ – UNL – CONICET, Santiago del Estero 2654, Santa Fe S3000AOJ, Argentina

ARTICLE INFO

Article history:
Available online 7 November 2011

Keywords:
Diesel soot
Oxidation kinetics
Cerium oxide
Reaction mechanism

ABSTRACT

In this work, a reaction mechanism for the catalytic combustion of diesel soot on cerium oxide is proposed. Kinetic results and catalyst characterization by Fourier-transformed Infra-Red spectroscopy (FTIR), X-ray Photoelectron Spectroscopy (XPS), Scanning Electron Microscopy (SEM), X-ray Diffraction Spectroscopy (XRD), and high frequency CO_2 pulses are used to obtain such mechanism. Temperature-programmed-oxidation experiments carried out up to intermediate temperatures made it possible to detect a transient kinetic response, in which a maximum in reaction rate at constant temperature was observed. This behavior is explained taking into account the amount of peroxides formed on the ceria surface. As the calcination temperature increases (from 400 to 800 °C), the amount of cerium superoxide and peroxide increases, thus accelerating the soot combustion reaction. These compounds were detected by FTIR. A higher total oxygen concentration on the ceria surface was detected by XPS on the catalyst calcined at high temperature. Carbon dioxide is not adsorbed on this support. The proposed reaction mechanism involves the formation of superoxides and peroxides. The latter are the active species that react with soot. These steps are strongly affected by temperature, being it possible to explain the kinetic results with this mechanism.

1. Introduction

Ceria is one of the most extensively used catalytic components in many after treatment technologies. CeO_2 is used in three-way catalysts for carbon monoxide, hydrocarbons and nitrogen oxides abatement, both as a fuel-borne catalyst and in the catalytic soot filters to eliminate these emissions [1]. It is well known that the main role of ceria is to provide oxygen-buffering capacity during the rich/lean oscillations of exhaust gases [2]. These oscillations only occur in Otto engines since in Diesel engines the operating conditions are always in lean regime (oxygen excess). The oxygen buffering capacity also known as oxygen storage capacity (OSC) derives from the easy and reversible CeO_2 reduction to CeO_{2-X}, where X can take values from 0 to 0.5. This oxygen loss yields non-stoichiometric structures, deficient in oxygen. Even after the lattice oxygen is removed with the consequent formation of a large number of oxygen vacancies, ceria retains its fluorite crystal structure [2], in which each Ce^{4+} cation is surrounded by eight O^{2-} ions forming the corners of a cube, and each O^{2-} is coordinated to four Ce^{4+} [3]. This facilitates rapid and complete refilling of oxygen vacancies upon exposure of CeO_{2-X} to oxygen, with the recovery of CeO_2 [2]. When cerium is reduced ($Ce^{4+} \rightarrow Ce^{3+}$), defects are generated around the Ce^{3+} cation. These defects are compensated with oxygen vacancies [4]. The property that facilitates the rapid and repeatable redox cycles is the facile creation, healing and diffusion of oxygen vacancies, especially at the ceria surface [5]. Hibino et al. [6] studied cation-doped ceria as a solid oxide fuel cell, working with hydrocarbon–air mixtures. In this paper, they found that this material has a very good ionic conduction and that it behaves as pure ionic conductor. This is in agreement with the results reported by Bueno-López et al. [7], who showed that the substitution of Ce^{4+} by Zr^{4+} or La^{3+}, favors the creation of structural defects, accelerates oxygen diffusion and induces more surface active oxygen species.

In this work, ceria calcined at 450 °C, 600 °C and 800 °C is studied. The objective is to visualize the phenomena that take place during soot combustion and to analyze the calcination temperature effect on these phenomena. The results here obtained are important to understand the role of CeO_2 in the reaction mechanism during soot combustion. Samples of ceria calcined at different temperatures were characterized by Fourier-transformed Infra-Red spectroscopy (FTIR), X-ray Photoelectron Spectroscopy (XPS),

* Corresponding author. Tel.: +54 342 453 3858; fax: +54 342 453 1068.
E-mail address: querini@fiq.unl.edu.ar (C.A. Querini).

1381-1169/$ – see front matter © 2011 Elsevier B.V. All rights reserved.
doi:10.1016/j.molcata.2011.10.018

Scanning Electron Microscopy (SEM), and X-ray Diffraction Spectroscopy (XRD). Activity tests were carried out to evaluate these catalysts in catalytic soot combustion.

2. Experimental

2.1. Catalysts and soot preparation

The catalysts used were commercial cerium (IV) oxide 99.9% (Aldrich) calcined at 450 °C, 600 °C and 800 °C during 2 h. These samples are labeled as CeO_2^{450}, CeO_2^{600} and CeO_2^{800}, respectively.

Soot was obtained by burning commercial diesel fuel as described in [8]. The soot was collected from the recipient walls and then dried in a stove at 120 °C during 24 h.

2.2. Catalyst activity

The catalytic activity was determined by temperature-programmed oxidation tests (TPO), carried out with catalyst:soot mixtures.

In this work, catalysts:soot mixtures were prepared with a mass ratio of 20:1. To prepare these mixtures, the weighted solids were placed in a mortar and were mechanically mixed for 6 min (tight contact). This contact mode is used in this study to understand the fundamentals of this quite complex reaction system. In addition, several experiments were carried out under loose contact conditions. In this case, the catalyst and the soot were mixed shaking both solids in a vial.

The amount of sample loaded into the reaction cell was 10 mg. The heating rate was 12 °C/min. A second set of experiments consisted in heating the sample at 12 °C/min until a given pre-selected temperature was reached, and then holding this temperature for a given time. Finally, another set of TPO experiments was carried out heating the sample in an inert gas flow (N_2) until a given temperature was reached. At this moment the gas was switched to an O_2/N_2 mixture holding a constant temperature. In all cases, the gas flow rate and composition were 40 ml/min and 5% O_2 (N_2 to balance), respectively. The gases coming out of the reaction cell went through a methanation reactor where the CO and CO_2 were converted to CH_4 with 100% conversion [9]. This reactor operated at 400 °C, and was loaded with a nickel catalyst. Methane formed in this reactor was continuously monitored with a Flame-Ionization Detector (FID).

With a heating rate of 12 °C/min, 5% O_2 composition in gas phase, 40 ml/min gas flow rate and 10 mg of catalyst:soot mass (20:1 ratio), the reaction proceeds under a kinetic controlled regime, as demonstrated in a previous work [10].

2.3. Catalyst characterization

The Brunauer–Emmett–Teller (BET) surface area of each catalyst was measured after calcination at different temperatures and prior to TPO experiments using a Quantachrome Autosorb 1 sorptometer.

Catalyst samples prior to be used in TPO experiments, and soot–catalyst mixtures after complete or partial burnt experiments at different final temperatures were characterized by Fourier Transform Infra-Red spectroscopy (FTIR). Infrared spectra were obtained using an IRPrestige-21 Shimadzu spectrometer. Samples were prepared in the form of pressed wafers (ca. 1% sample in KBr). All spectra involved the accumulation of 80 scans at 8 cm^{-1} resolution.

Crystalline phases of fresh catalysts were identified by powder X-ray diffraction (XRD) analysis using a Shimadzu XD-D1 diffractometer, equipped with a CuKα radiation source and using a scanning rate of 1 min^{-1}. The crystallite size (D) was estimated using Scherrer's equation:

$$D = \frac{K \cdot \lambda}{\beta \cdot \cos\theta}$$

where λ is the wavelength of the radiation used, β is the full width at half maximum of the diffraction peak considered, K is a shape factor and θ is the diffraction angle at which the peak appears.

The morphology of soot-catalyst mixtures, both just prepared and after partial burnt experiments, were examined by Scanning Electron Microscopy (JEOL JSM 35C) operated at 20 kV.

X-ray Photoelectron Spectroscopy (XPS) studies were carried out with a Specs multi-technique instrument. It is equipped with an X-ray non-monochromatic source (Mg/Al dual anode) and a hemispheric analyzer PHOIBOS 150 that operates in fixed transmission mode (FAT). Spectra were obtained with pass energy of 30 eV and an Al anode (radiation Al K_α 1486.6 eV) operating at 100 W. The pressure in the analysis camera during the measurement was lower than 2×10^{-9} mbar. For each sample the spectra taken corresponds to energy levels of Ce 3d, O 1s and C 1s. Binding energies were referred to the Ce $3d_{3/2}$ u‴ signal (916.6 eV). Peak fitting and background contribution were made with apparatus software. Quantitative analyses were done using appropriate Scofield factors. It has to be mentioned that after the calcination step, the samples were exposed to the environment, and then introduced in the XPS analysis chamber and treated under high vacuum. During this handling and treatment, the catalyst surface may change. However, all the samples have been treated with the same procedure and, therefore, the results are useful to compare the effect of the different treatments on the surface composition.

The CO (or CO_2) interaction with the catalyst:soot mixture was analyzed by high frequency CO (or CO_2) pulses. This technique was previously used in other studies [11–14]. This technique consists in sending CO (or CO_2) pulses at a frequency of 0.1 Hz. When pulses were sent to the catalyst, the gas carrier used contained 5% O_2 (N_2 to balance), and when pulses were sent to catalyst:soot mixtures, the gas carrier used was N_2 to avoid soot combustion at high temperature. Pulses series were sent at different temperatures, which were chosen in the range in which the maximum in the TPO profile was observed. As the strength of the interaction between the catalyst and the CO_2 increases, the amplitude of the pulses coming out of the cell decreases.

Since the methanation reactor does not distinguish between CO_2 or CO, a set of CO pulses were carried out with a silicagel column before the methanation reactor in order to separate CO from CO_2. In this case, the pulses were sent to the catalyst every 2 min, the rest of conditions being the same as those used in the high frequency pulses experiments.

3. Results and discussion

3.1. Activity tests

Fig. 1 shows curves of conversion vs. temperature for catalytic and non-catalytic combustion. The conversion is defined as:

$$x = \frac{C_0 - C}{C_0}$$

where C_0 is the initial total soot concentration, and C is the amount of soot left on the catalyst after burning by heating up to a given T value. Both concentrations are calculated using the total area and the area up to a given T value respectively, obtained from the TPO profile.

To obtain the values corresponding to the non-catalytic combustion rates, soot has been mixed with SiO_2 using the same proportion

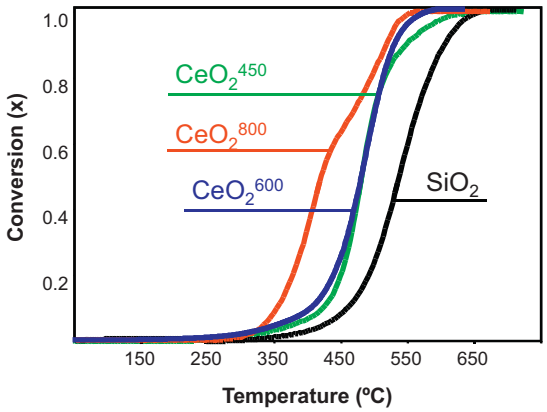

Fig. 1. Conversion vs. temperature curves, calculated from TPO experiments carried out at 12 °C/min.

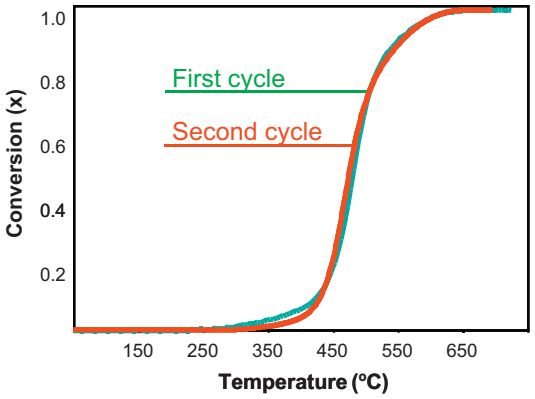

Fig. 2. Successive combustion cycles with CeO_2^{450}.

as in the case of CeO_2. The mixtures were heated from room temperature up to 700 °C (approximately) at constant heating rate (12 °C/min). In all cases, complete soot conversion was reached. This was verified by running a second TPO up to higher temperatures, right after cooling the sample at the end of the experiment shown in Fig. 1. It can be seen that ceria calcined at 450 °C has a similar behavior that the one calcined at 600 °C. The maximum reaction rate was observed at 380 °C with CeO_2^{800}, and at 480 °C with CeO_2^{450} and CeO_2^{600}, as compared with 530 °C registered for non-catalytic combustion. These temperatures correspond to the inflexion point in each curve shown in Fig. 1. This figure also shows differences among the conversion curves. Profiles corresponding to CeO_2^{450} and CeO_2^{600} are similar and both have one inflexion point at the temperature mentioned above. Instead of this, the curve corresponding to CeO_2^{800} has two inflexion points, one at 380 °C, and the other at 480 °C, which corresponds to a local maximum. In Table 1 characteristic temperatures are listed. TI is the temperature at which combustion begins, TM is the temperature at which maximum reaction rate is registered, and TF is the temperature at which carbonaceous materials are completely converted. These results clearly indicate that the combustion of carbonaceous material is produced mainly by the oxygen provided by ceria and not directly by molecular oxygen from the gas phase. The experimental evidence of this affirmation is given in Fig. 1. At a given temperature, for example 500 °C, the conversion value for non-catalytic combustion is approximately 0.2, whereas for the catalytic combustion the conversion reaches values around 0.7 for CeO_2^{450} or CeO_2^{600}, and 0.85 for CeO_2^{800}. This indicates that the catalytic combustion with surface oxygen, proceeds with higher velocity than the non-catalytic combustion, with molecular oxygen. This is in agreement with previous reports from other authors [7]. However, in a carbothermic reduction of the catalyst:soot mixture, carried out heating the sample in an inert atmosphere, it was found that CeO_2 cannot supply all the oxygen needed to eliminate all the carbonaceous material (not shown). CeO_2^{450} and CeO_2^{800} eliminated approximately 8% and 28% of the soot that was mixed with the catalyst, respectively. Therefore, CeO_2^{800} supplied more active oxygen for soot combustion than CeO_2^{450}. This evidence agrees with results shown in Fig. 1. Therefore, particulate matter reacts with oxygen from the support, but the presence of molecular oxygen in the gaseous phase is necessary for the combustion to proceed. Mul et al. [15] suggested that molecular oxygen is necessary to maintain a chemical potential gradient to 'push the chain of surface oxygen atoms'.

Fig. 2 displays two consecutive combustion cycles for the catalyst calcined at 450 °C. The spent catalyst after a TPO experiment was mixed with soot and a second TPO was carried out. It can be seen that the catalyst do not loose activity, since the combustion curves obtained in the first and in the second TPO are very similar. The characteristic temperatures are the same in both reaction cycles.

TPO carried out with loose contact mixtures (not shown) demonstrates that the combustion takes place at temperatures higher than with tight contact. These results are in agreement with those reported in a previous work [8] and by other authors [16]. The characteristic temperatures are listed in Table 1. It can be seen that TI and TM values are a few degrees below the respective temperatures for non-catalytic combustion. Moreover, there are no differences between the characteristic temperatures obtained in loose contact mode with cerium oxide calcined at 450 or 800 °C. Therefore, with this catalyst a high percentage of the soot combustion takes place by a non-catalytic pathway in the case of a loose contact between the soot and the catalyst.

FTIR spectra were taken to catalysts samples after and before being used in complete TPO experiments. Fig. 3 shows these results. It can be seen that there are differences among the spectra. The catalysts calcined at 450 and 600 °C, show bands that are assigned to water (1650 cm^{-1}) [17] and superoxides (1125 cm^{-1}) [18–20]. The latter band is more intense for CeO_2^{600} than CeO_2^{450}. The spectrum corresponding to CeO_2^{800}, is different from those calcined at lower temperatures. In the case of catalyst calcined at 800 °C, in addition to the bands that correspond to water and peroxides, the spectrum shows the characteristics bands that are assigned to surface carbonate at 1450, 1375, 1050, 850 and 705 cm^{-1} [21]. Another band that appears in this catalyst is the one observed at 883 cm^{-1}, which is assigned to peroxides [18–20]. The spectrum taken after one combustion cycle for catalyst CeO_2^{450} (spectrum identified as $CeO_2^{450\ 1st\ cycle}$), is very similar to the spectrum corresponding to fresh catalyst CeO_2^{600}. This result is reasonably, since the combustion was carried out up to 650 °C. The spectra taken after the second combustion cycle with CeO_2^{450} and first combustion cycle with

Table 1
Characteristic temperatures for catalytic soot combustion using CeO_2^{450}, CeO_2^{600} and CeO_2^{800} as catalysts, obtained from TPO profiles. Heating rate: 12 °C/min.

	TI (°C)	TM (°C)	TF (°C)
SiO_2	350	530	630
CeO_2^{450} TC	280	480	630
CeO_2^{600} TC	280	480	630
CeO_2^{800} TC	230	380[a]	550
CeO_2^{450} LC	325	520	630
CeO_2^{800} LC	315	515	630

TC, tight contact; LC, loose contact.
[a] Correspond to absolute maximum reaction rate.

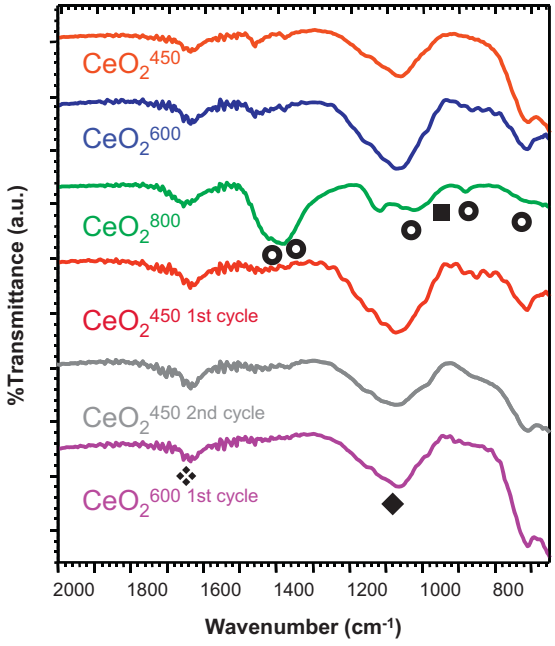

Fig. 3. FTIR spectra for catalysts calcined at different temperatures and after TPO tests. ❖ water; ○ surface carbonates; ■ peroxides; ♦ superoxides.

$CeO_2{}^{600}$, labeled in Fig. 3 as $CeO_2{}^{450\ 2nd\ cycle}$ and $CeO_2{}^{600\ 1st\ cycle}$ respectively, are very similar between them.

These results are in agreement with those shown in Figs. 1 and 2, since the catalysts calcined at 450 °C and 600 °C have similar activity, and also because successive combustion cycles do not lead to any change in catalytic activity for catalyst calcined at 450 °C.

Substoichiometric ceria (CeO_{2-X}) is produced upon oxygen elimination from the oxide surface and the subsequent formation of oxygen vacancies. The re-oxidation process by molecular oxygen may proceed according to the following scheme [18]:

$$O_{2(g)} \rightleftarrows [O_{2(ads)}] \underset{-e^-}{\overset{+e^-}{\rightleftarrows}} [O^-_{2(ads)}] \underset{-e^-}{\overset{+e^-}{\rightleftarrows}} [O^{2-}_{2(ads)}] \rightleftarrows [2O^-_{(ads)}] \underset{-e^-}{\overset{+e^-}{\rightleftarrows}} [2O^{2-}_{lattice}]$$

In a first step, the molecular oxygen ($O_{2(g)}$) present in the gas phase is adsorbed on the ceria surface ($O_{2(ads)}$). Then, the adsorbed oxygen is transformed in superoxide species ($O_{2(ads)}{}^-$) and then in peroxides ($O_{2(ads)}{}^{2-}$). The next two steps describe the incorporation of oxygen to the bulk oxide ($O_{lattice}{}^{2-}$). It has been proposed that $O_2{}^-$ and $O_2{}^{2-}$ are reaction intermediaries in catalytic soot combustion [14,22]. Teranishi et al. [23] investigated the formation of active oxygen by electrochemical oxidation of H_2O vapor, coupled with carbon detection using those oxygen species, by utilizing $Sn_{0.9}In_{0.1}P_2O_7$ as a proton conductor and Pt as an electrocatalyst. They found that this oxygen species showed high activity for carbon oxidation.

The peroxides can reach the carbon atoms by surface diffusion or by spill-over. Peroxides react with carbon atoms that are in the solid–solid interface (carbon in contact with catalyst) by surface diffusion. Also, it is possible that the peroxides react with carbon atoms that are in the solid–gas interface (carbon that is in contact with gaseous phase) by spill-over. In loose contact, most of the carbon atoms are in contact with gaseous phase and, consequently, the combustion process takes place mainly by spill-over. This could be the reason why catalysts calcined at different temperatures have the same catalytic behavior in loose contact.

Catalysts were analyzed by XRD. The diffractograms are shown in Fig. 4. It can be seen that the crystalline phase was not affected by thermal treatment at high temperature. Ceria calcined at both low and at high temperature displays a similar diffractogram. The

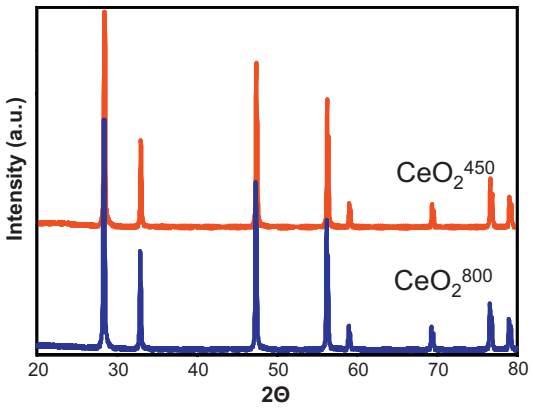

Fig. 4. XRD patterns of ceria calcined at different temperatures.

signals that can be seen correspond to typical reflections of the cubic structure face centered at 2Θ: 28.5°, 33.1°, 47.6°, 56.5°, 59.2°, 69.5°, 76.8° and 79.1°. These signals correspond to the planes (1 1 1), (2 0 0), (2 2 0), (3 1 1), (2 2 2), (4 0 0), (3 3 1) and (4 2 0), respectively (card JCPDS-ICDD 78-694 Rad. CuKα_1). The calculated crystal sizes are 355 Å and 398 Å for $CeO_2{}^{450}$ and $CeO_2{}^{800}$, respectively. Therefore, the temperature treatment affects neither the crystalline phase nor the crystal size.

SEM micrographs taken to ceria calcined at 450 and 800 °C are shown in Fig. 5. Certain differences can be observed between $CeO_2{}^{450}$ and $CeO_2{}^{800}$ (Fig. 5A and B, respectively). The ceria calcined at low temperature does not present evidence of surface sintering; the morphology observed is typical of cerium oxide. On the

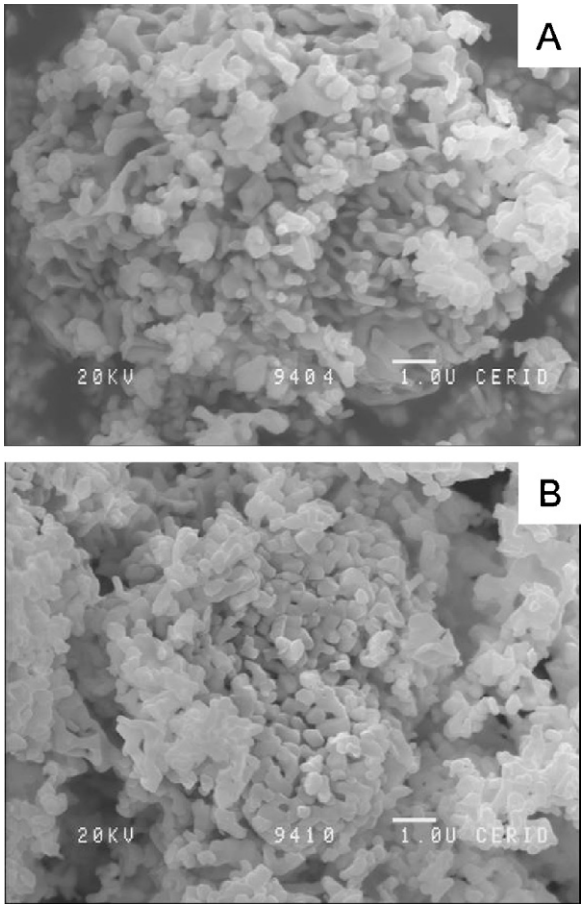

Fig. 5. SEM micrographs of $CeO_2{}^{450}$ (A) and $CeO_2{}^{800}$ (B).

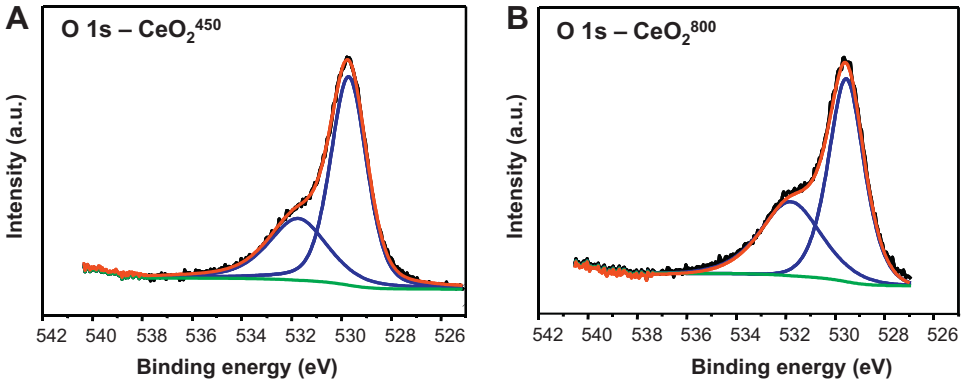

Fig. 6. X-ray photoelectron spectra in the O 1s region. (A) CeO_2 calcined at 450 °C and (B) CeO_2 calcined at 800 °C.

other hand, ceria calcined at high temperature shows zones that apparently underwent a sintering process. Nevertheless, according to these pictures there are no major changes in crystal size, as seen by XRD. This is in agreement with BET surface area results, the values measured for all catalysts are similar and they are in the order of 20 $m^2\ g^{-1}$.

XPS spectra were taken to the catalysts calcined at different temperatures. The binding energy range analyzed was that corresponding to Ce 3d, O 1s and C 1s. Fig. 6 shows the O 1s spectra obtained with catalysts calcined at 450 and 800 °C (Fig. 6A and B, respectively). Table 2 shows the surface atomic ratios calculated from XPS data. The oxygen present on the surface in any form (carbonates, peroxides, superoxides) is indicated in this table as O_{ads}. The bulk oxygen is O_{ret}, and represents the oxygen that forms part of the crystal structure of cerium oxide. This distinction can be done because both kinds of oxygen have different binding energies: 529.15 eV for O_{ret} and 531.3 eV for O_{ads}. It can be seen that the oxide calcined at higher temperature has a higher O_{ads} percentage in comparison with the oxide calcined at lower temperature. This can be the reason for the better activity of the catalyst calcined at higher temperature. In the same table, it can also be seen that Ce^{3+} percentage is lower in the catalyst calcined at 800 °C than in the catalyst calcined at 450 °C. Consequently, the O_{ads}/Ce^{3+} ratio is higher for the catalyst calcined at higher temperature.

High frequency CO_2 pulses made at different temperatures (not shown), between 280 and 580 °C, demonstrated that the adsorption–desorption processes occurs at the same average rate as the pulse injection, both with $CeO_2{}^{450}$ or $CeO_2{}^{800}$. For both catalysts, the pulse amplitude is the same as in the blank experiment (pulses sent with an empty cell, where there is no interaction). Similar results were obtained when pulses were carried out with CO. This suggests that in this case, a reaction pathway involving the intermediate compound with CO_2 (such as carbonates) is not making an important contribution to the overall reaction rate. The mechanism involving these types of intermediates has been previously proposed for catalysts containing alkaline metals [24].

CO pulses with the silicagel column previous to the methanation reactor reveal that the cerium oxide is capable to oxidize the CO to CO_2. This capability is also affected by calcination temperature. Fig. 7 shows pulses sent at different temperatures with $CeO_2{}^{450}$. It can be seen that at high temperatures, in the 400–550 °C range, the amount of CO_2 produced is significant, but when the temperature is

Table 2
Surface atomic ratios determined by XPS.

	% O_{ads}	% O_{ret}	% Ce^{3+}	O_{ads}/Ce^{3+}
$CeO_2{}^{450}$	34.34	65.66	11.29	3.04
$CeO_2{}^{800}$	38.16	61.84	10.08	3.78

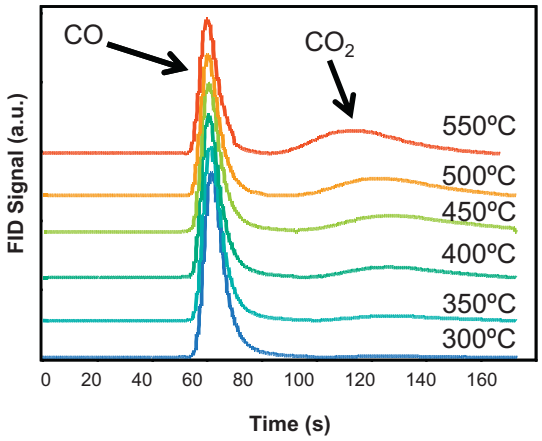

Fig. 7. CO pulses sent over $CeO_2{}^{450}$ at different temperatures.

lower the CO conversion into CO_2 is also very low. Table 3 displays the percentages of unreacted CO and the CO converted CO_2, calculated for each temperature. When this experiment was carried out with $CeO_2{}^{800}$, the CO_2 yield is higher at higher temperatures as can be seen in Table 3. In the same table, it can be seen that for the same temperature the CO conversion with $CeO_2{}^{800}$ is higher than with the $CeO_2{}^{450}$. These results are in agreement with those shown in Fig. 1. The catalyst calcined at 800 °C supplied more active oxygen for oxidation process than the calcined at 450 °C.

3.2. Partial burnt tests

Another set of TPO experiments was carried out heating the sample at 12 °C/min up to a given temperature. This temperature was selected in the range TI–TM values (see Table 1). Once this temperature was reached, it was kept constant until the reaction rate decreased to zero. This experimental design makes it possible to observe phenomena that cannot be detected with conventional

Table 3
percentages of unreacted CO and produced CO_2 during CO pulses sent at different temperatures to CeO_2 catalyst calcined at different temperatures.

T (°C)	$CeO_2{}^{450}$		$CeO_2{}^{800}$	
	% CO	% CO_2	% CO	% CO_2
550	55.9	44.1	27.51	72.49
500	65.66	34.34	50.18	49.82
450	68.53	31.47	68.11	31.89
400	79.38	20.62	76.65	23.35
350	89.42	10.58	79.82	20.18
300	96.99	3.01	80.50	19.50

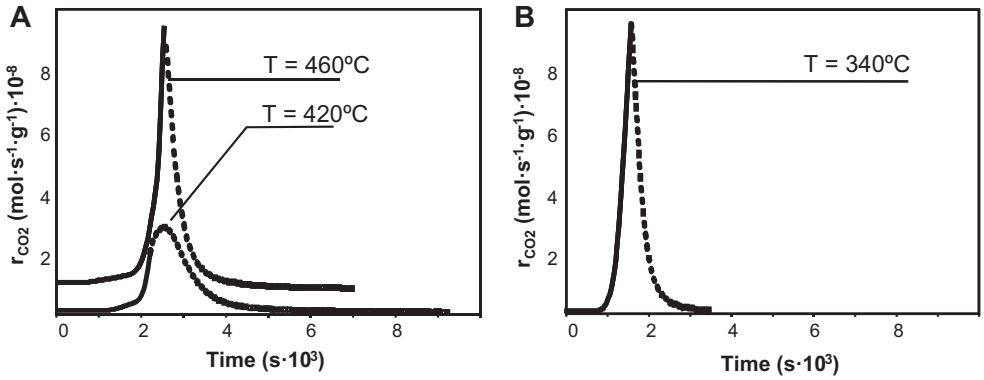

Fig. 8. TPO analysis up to different final temperatures. Full line heating at 12 °C/min, dotted line isothermal conditions at indicated temperature. (A) $CeO_2{}^{450}$ and (B) $CeO_2{}^{800}$.

TPO analysis. Fig. 8A and B presents the reaction rate vs. time, corresponding to ceria calcined at 450 °C and 800 °C, respectively. Fig. 8A shows that under isothermal conditions with $CeO_2{}^{450}$, the reaction rate goes through a maximum, depending upon the final temperature selected for the experiment. Our group has already reported this kind of behavior with catalysts prepared with potassium supported on ceria [14]. This phenomenon cannot be seen at temperatures closer to TI (not shown) or even at temperatures closer to the TM value. Fig. 8B shows the results obtained with $CeO_2{}^{800}$, when the temperature was kept constant at 340 °C. It is necessary to remark that experiments carried out at different temperatures between TI and TM with $CeO_2{}^{800}$ gave the same result, i.e., once the isothermal condition was reached, the reaction rate decays following an exponential curve. The spent catalyst was mixed again with soot and a second partial burnt experiment was carried out. The results are shown in Fig. 9. It can be seen that in the second cycle the catalyst has the same behavior, i.e., under isothermal condition the reaction rate keeps increasing, reaches a maximum and then decreases in an exponential way.

This increase in the reaction rate at constant temperature is not associated with a runaway phenomenon. We have previously demonstrated that under the experimental conditions used in these catalytic tests (catalyst:soot ratio, heating rate, gas flow, mass loaded into the cell, etc.) there are no mass or energy transfer limitations [8]. Additionally, we have recently addressed the runaway phenomenon, and shown the TPO profiles observed under this condition [25]. When the reaction goes into an energy-transfer limitation regime, the TPO profile displays a sharp peak. In the experiments reported in this paper, the typical shape found when the runaway takes place was not observed.

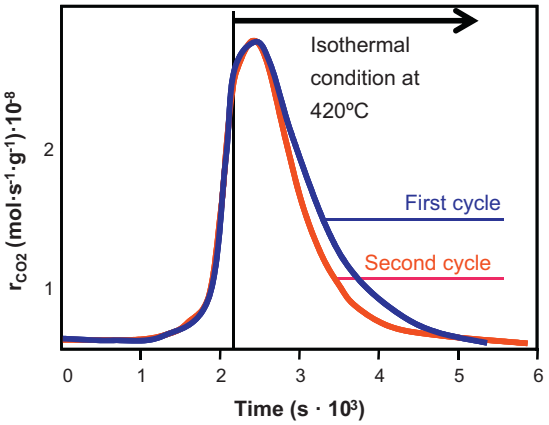

Fig. 9. Partial burnt successive tests for catalyst calcined at 450 °C.

Catalyst:soot mixtures were analyzed by FTIR before and after partial burnt experiments. The mixture was heated up to a given temperature, and then quickly cooled down to ambient temperature. The spectra obtained with these samples are shown in Fig. 10. These results indicate that there are different species on the ceria surface depending if it is calcined at 450 °C or at 800 °C, as was previously shown in Fig. 3. This is the reason of the different catalytic behavior for these two catalysts, as shown in Fig. 8. Fig. 10A shows the spectra obtained with catalyst:soot mixtures using $CeO_2{}^{450}$. Spectrum (a) corresponds to the catalyst:soot mixture as prepared. In this spectrum, it can be seen that there are no signals that can be assigned to soot. In other words, soot does not present absorption bands in the wave number range analyzed. In the same figure, the other spectra show that the higher the temperature used to remove the soot, the more intense the absorption bands in certain regions of the spectra. In this case, bands assigned to water (1650 cm^{-1}) [16] and superoxides (O_2^-) (1125 cm^{-1}) can be identified [18–20]. The spectra corresponding to ceria calcined at 800 °C (Fig. 10B) as previously said, are very different from those shown in Fig. 10A. The spectra shown in Fig. 10B have well defined signals at 1650, 1450, 1375, 1125, 1050, 883, 850 and 705 cm^{-1}. The band that appears at 1650 cm^{-1} is assigned to water and the band at 1125 cm^{-1} is assigned to superoxides. The signals at 1450, 1375, 1050, 850 and 705 cm^{-1} that do not appear in $CeO_2{}^{450}$, are attributed to surface carbonates [21]. Another band that does not appear in the metal oxide calcined at lower temperature is the one observed at 883 cm^{-1} assigned to peroxides ($O_2{}^{2-}$) [18–20]. In agreement with XPS results, these results indicate that there is an increase in the availability of superoxides and peroxides as the calcination temperature increases, and also as the temperature is increased during the reaction with soot. The latter is very important from the mechanistic point of view, because it indicates that these compounds would be playing a key role in the reaction pathway.

3.3. Kinetic parameters

Isothermal combustions at different temperatures were carried out in order to determine the global activation energy (E). Similarly to what was reported in a previous work [14], a global combustion reaction is considered, with a power law kinetic expression. In this way, it is possible to estimate the activation energy (E) as a global value by using the expression:

$$\ln(r) = \ln(A) + \ln(f(C,P)) - \frac{E}{R}\frac{1}{T}$$

where 'r' is the reaction rate, 'A' is the pre-exponential factor, '$f(C,P)$' is a function that includes the dependence of reaction rate with soot concentration, soot particle geometry and oxygen partial pressure, 'E' is the global activation energy, 'R' is the gases universal constant

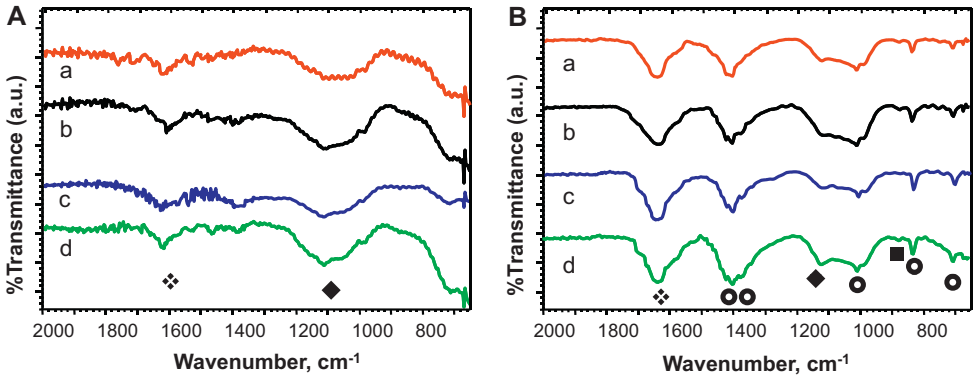

Fig. 10. FTIR spectra for catalyst:soot mixtures. (A) $CeO_2{}^{450}$; (a) catalyst:soot mixture; partial burnt at: (b) 400 °C, (c) 420 °C, (d) 440 °C. (B) $CeO_2{}^{800}$; (a) catalyst soot mixture; partial burnt at: (b) 305 °C, (c) 310 °C, (d) 315 °C. ❖ water; ❍ surface carbonates; ■ peroxides; ♦ superoxides.

Table 4
Global activation energies for different conversion levels calculated from the experiments shown in Fig. 11.

x	E (kcal/mol)		A (s^{-1} atm^{-1})	
	$CeO_2{}^{450}$	$CeO_2{}^{800}$	$CeO_2{}^{450}$	$CeO_2{}^{800}$
0.1	27.17 ± 1.8	22.80 ± 1.5	62.04 ± 4.14	26179 ± 1745
0.2	27.44 ± 1.8	20.99 ± 1.4	75.52 ± 5.07	$1.73 \times 10^{11} \pm 1.15 \times 10^{10}$
0.3	28.04 ± 1.9	25.05 ± 1.7	121.25 ± 8.08	$1.09 \times 10^{8} \pm 7.3 \times 10^{7}$
0.4	26.37 ± 1.7	23.41 ± 1.6	38.39 ± 2.56	$2.65 \times 10^{7} \pm 1.7 \times 10^{6}$
0.5	24.00 ± 1.6	20.84 ± 1.4	7.26 ± 0.49	$9.37 \times 10^{5} \pm 6.25 \times 10^{4}$
0.6	21.63 ± 1.4	19.35 ± 1.3	1.34 ± 0.09	$3.11 \times 10^{6} \pm 2.07 \times 10^{5}$
0.7	18.53 ± 1.2	16.79 ± 1.1	0.14 ± 0.01	$1.09 \times 10^{5} \pm 7.26 \times 10^{3}$
0.8	14.70 ± 1.0	5.84 ± 0.8	$9.00 \times 10^{-3} \pm 6 \times 10^{-4}$	19.25 ± 1.29
0.9	5.10 ± 0.3	1.68 ± 0.3	$9.64 \times 10^{-6} \pm 7 \times 10^{-8}$	0.29 ± 0.02

and 'T' the absolute temperature. Fig. 11 shows the conversion as a function of time obtained with $CeO_2{}^{450}$. Experiments with $CeO_2{}^{800}$ were carried out at 330, 350, 370 and 390 °C (not shown). Table 4 shows the global activation energy values (E) and pre-exponential factor (A) calculated for both catalysts at different conversion levels.

Two important facts can be pointed out regarding data shown in Table 4. The first one is that the E value changes for both catalysts as the conversion increases. This indicates that the reaction mechanism is complex, with more than one step involved in the mechanism. This change in the activation energy also clearly shows that the controlling step or the relative rates of the different steps vary with the advancement of the reaction. Krishna et al. reported a similar behavior on the activation energy values [1]. This variation is very important and it is something to take into account when comparing data reported by different groups. For example, different values have been reported, such as 33.92 kcal/mol [26], and 37.07 kcal/mol [22], in both cases for catalytic combustion of soot with CeO_2. However, the conversion levels for which these values were determined are not reported. Another interesting result shown in Table 4 is that the activation energy is smaller in the case of $CeO_2{}^{800}$ as compared with the corresponding value obtained with $CeO_2{}^{450}$, in agreement with results shown in Fig. 1. The different catalytic behavior observed in Fig. 1 (one or two inflexion points for $CeO_2{}^{450}$, $CeO_2{}^{600}$ or $CeO_2{}^{800}$ respectively), are due to the different surface compositions obtained at different calcination temperatures. Depending upon the concentration of intermediate species, and their changes with the temperature and reaction time, the soot can be burn by different reaction pathways, thus leading to more than one peak in the TPO profile or more than one inflexion point in the conversion vs temperature curves. The better activity of $CeO_2{}^{800}$ compared with $CeO_2{}^{450}$ correlates with this lower activation energy. The pre-exponential factor is higher in the case of $CeO_2{}^{800}$, which also agrees with the concept presented in this work, i.e. that the CeO_2 calcined at high temperature (800 °C) has a higher number of active sites thus increasing the rate of collisions between the active oxygen (peroxides) and the soot.

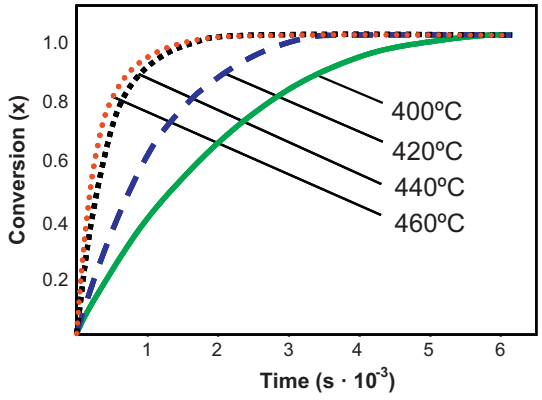

Fig. 11. Isothermal combustion at different temperatures. $CeO_2{}^{450}$.

3.4. Reaction mechanism

With the experimental evidence shown above, it can be proposed that during the catalytic soot combustion on CeO_2, the following steps take place:

- oxygen adsorption on ceria surface
- superoxide and peroxide formation
- reaction of peroxide with soot and formation of carbon dioxide
- diffusion of oxygen vacancies

In the first step, the oxygen is adsorbed on the cerium oxide to give superoxide species on the surface. Even though the adsorption is a reversible process, in this case it is considered that the reaction

rate between active oxygen species and soot is much faster than the reaction in which active oxygen species decompose forming molecular oxygen [7]. Consequently, the reaction is considered as irreversible. This hypothesis was verified by comparison of the fitting capacity of each of these models, and mainly by its capacity to predict the kinetic response under different experimental conditions.

$$nCeO_x + O_2 \rightarrow [nCeO_x]^{+}O_2^{-} \quad (1)$$

Through electronic diffusive phenomena, the superoxide is transformed into peroxide ions. The superoxide can also be converted into the oxidized form of cerium oxide, the subscript '*y*' being greater than '*x*'. Electrons have high mobility; therefore, these steps are proposed to be reversible.

$$[nCeO_x]^{+}O_2^{-} \leftrightarrow [nCeO_x]^{2+}O_2^{2-} \quad (2)$$

$$[nCeO_x]^{+}O_2^{-} \leftrightarrow nCeO_y \quad (3)$$

Peroxides provide the active oxygen that reacts with soot to give adsorbed carbon dioxide.

$$[nCeO_x]^{2+}O_2^{2-} + C \rightarrow [nCeO_x]^{2+}[CO_2]^{2-} \quad (4)$$

Then, the carbon dioxide desorbs leaving an oxygen vacancy. According to the experimental evidence obtained with high frequency CO_2 pulses, it is considered that carbon dioxide does not adsorb over the cerium oxide surface.

$$[nCeO_x]^{2+}[CO_2]^{2-} \rightarrow [nCeO_x]^{2+}[\ ]^{2-} + CO_2 \quad (5)$$

In this way, the latter two steps can be condensed into the next expression:

$$[nCeO_x]^{2+}O_2^{2-} + C \rightarrow [nCeO_x]^{2+}[\ ]^{2-} + CO_2 \quad (6)$$

Finally, the oxygen vacancies spread out to yield reduced sites where the molecular oxygen adsorbs:

$$[nCeO_x]^{2+}[\ ]^{2-} \rightarrow nCeO_x \quad (7)$$

Since the high frequency CO_2 pulses did not show an interaction of this gas with soot (not shown), the direct reaction between soot and carbon dioxide is not considered. In other words, the following reaction does not take place in the temperature range of interest in this analysis:

$$C + CO_2 \rightarrow 2CO \quad (8)$$

This reaction step has been proposed in several works for carbon combustion, e.g. [27].

Therefore, the reaction mechanism proposed for soot combustion on cerium oxide is represented by reactions (1)–(3), (6) and (7). This reaction mechanism makes it possible to explain the kinetic behavior shown in Fig. 8A. The soot oxidation involves the formation of superoxides and peroxides. For the catalyst calcined at 450 °C, the amount of these compounds is low, as indicated by the FTIR analyses. At low temperature (e.g., 420 °C), the maximum concentration of these intermediates is reached after some time and, therefore, the reaction rate increases according to the increase in the peroxide concentration. At higher temperatures, such as 460 °C, the maximum concentration of these intermediates has already been reached, and therefore the reaction rate at constant temperature decreases monotonically [14]. For the catalyst calcined at 800 °C, the intermediates are more easily formed (as seen in XPS and FTIR). Therefore, since the peroxide concentration has already reached the maximum and there is a decrease in the amount of soot, the reaction rate decreases with time.

Atribak et al. [28] studied the effect of yttrium and zirconium on cerium oxide activity for soot combustion. It was concluded that the improvement on the activity in tight contact mode was because the promoters enhanced oxygen mobility and surface reducibility. The mechanism we are proposing in this work includes these steps.

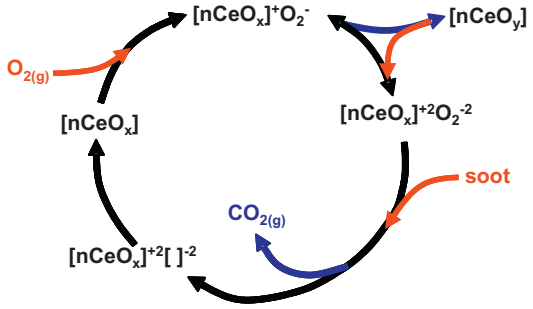

Scheme 1.

The reaction mechanism is summarized in Scheme 1.

4. Conclusions

It has been found that the cerium oxide calcined at higher temperatures has a better activity than the oxide calcined at lower temperature. According to FTIR and XPS results, this better activity is due to the higher concentration of superoxides and peroxides on the catalyst calcined at high temperature. These species provide active oxygen that reacts with soot to yield carbon dioxide.

Soot is burnt by the oxygen provided by ceria and not by molecular oxygen. Nevertheless, the presence of molecular oxygen is necessary in the gaseous phase to completely burn the soot. The reaction mechanism is complex, involving several steps. The formation of superficial oxygenated species, which strongly depends on the calcination and reaction temperatures, limits the reaction rate. Because of this, an increase in reaction rate at constant temperature is observed for the catalyst calcined at 450 °C. This phenomenon cannot be seen with the catalyst calcined at 800 °C because the formation of superoxides and peroxides is kinetically favored. The apparent activation energy obtained considering that the reaction takes place only in one step, decreases as the soot conversion increases, also indicating that the reaction mechanism involves several steps.

The carbon dioxide generated in soot combustion interacts neither with catalyst nor with the soot and, therefore, the reaction mechanism does not involve the formation of intermediates involving carbonates.

To improve the catalyst activity of ceria, it is necessary to add promoters that facilitate the formation of peroxides and oxygen vacancies. In addition, these compounds must diffuse throughout the surface, since these species are involved in the soot oxidation mechanism.

References

[1] K. Krishna, A. Bueno-López, M. Makkee, J.A. Moulijn, Appl. Catal. B 75 (2007) 189–200.
[2] A. Trovarelli, M. Boaro, E. Rocchini, C. De Leitenburg, G. Dolcetti, J. Alloys Compd. 323–324 (2001) 584–591.
[3] A. Gotte, D. Spanberg, K. Hermansson, M. Baudin, Solid State Ionics 178 (2007) 1421–1427.
[4] M. Mogensen, N.M. Sammes, G.A. Tompsett, Solid State Ionics 129 (2000) 63–94.
[5] M.V. Ganduglia-Pirovano, A. Hofmann, J. Sauer, Surf. Sci. Rep. 62 (2007) 219–270.
[6] T. Hibino, A. Hashimoto, T. Inoue, J. Tokuno, S. Yoshida, M. Sano, Science 288 (2000) 2031–2033.
[7] A. Bueno-López, K. Krishna, M. Makkee, J.A. Moulijn, J. Catal. 230 (2005) 237–248.
[8] C.A. Querini, M.A. Ulla, F. Requejo, J. Soria, U.A. Sedrán, E.E. Miró, Appl. Catal. B 15 (1998) 5–19.
[9] S.C. Fung, C.A. Querini, J. Catal. 138 (1992) 240–254.
[10] M.A. Peralta, M.S. Gross, B.S. Sánchez, C.A. Querini, Chem. Eng. J. 152 (2009) 234–241.
[11] V.G. Milt, M.L. Pisarello, E.E. Miró, C.A. Querini, Appl. Catal. B 41 (2003) 397–414.

[12] V.G. Milt, C.A. Querini, E.E. Miró, Thermochim. Acta 404 (2003) 177–186.
[13] M.L. Pisarello, V.G. Milt, M.A. Peralta, C.A. Querini, E.E. Miró, Latin Am. Appl. Res. 33 (2003) 345.
[14] M.S. Gross, M.A. Ulla, C.A. Querini, Appl. Catal. A 360 (2009) 81–88.
[15] G. Mul, F. Kapteijn, C. Doornkamp, J.A. Moulijn, J. Catal. 179 (1998) 258–266.
[16] R. Matarrese, L. Castoldi, L. Lietti, P. Forzatti, Catal. Today 136 (2008) 11–17.
[17] A. Davydov, in: N.T. Sheppard (Ed.), Molecular Spectroscopy of Oxide Catalyst Surfaces, John Willey & Sons Ltd., 2003, p. 72.
[18] C. Binet, M. Daturi, J.C. Lavalley, Catal. Today 50 (1999) 207–225.
[19] M. Daturi, E. Finocchio, C. Binet, J.C. Lavalley, F. Fally, V. Perrichon, H. Vidal, N. Hickey, J. Kaspar, J. Phys. Chem. B 104 (2000) 9186.
[20] V. Pushcarev, V. Kovalchuk, J. d'Itri, J. Phys. Chem. B 108 (2004) 534.
[21] A. Davydov, in: N.T. Sheppard (Ed.), Molecular Spectroscopy of Oxide Catalyst Surfaces, John Willey & Sons Ltd., 2003, p. 135.
[22] L. Zhu, J. Yu, X. Wang, J. Hazard. Mater. 140 (2007) 205–210.
[23] S. Teranishi, K. Kondo, A. Tsuge, T. Hibino, Sens. Actuators B: Chem. 140 (2009) 170–175.
[24] M.L. Pisarello, V. Milt, M.A. Peralta, C.A. Querini, E.E. Miró, Catal. Today 75 (2002) 465–470.
[25] M.A. Peralta, M.S. Gross, M.A. Ulla, C.A. Querini, Appl. Catal. A 367 (2009) 59–69.
[26] X. Wu, D. Liu, K. Li, J. Li, D. Weng, Catal. Commun. 8 (2007) 1274–1278.
[27] P. Kilpinen, S. Kallio, J. Konttinen, V. Barisic, Fuel 81 (2002) 2349–2362.
[28] I. Atribak, A. Bueno-López, A. García-García, J. Mol. Catal. A: Chem. 300 (2009) 103.